International Journal of Mechatronics and Applied Mechanics
2026, Issue 25, Vol. II

INTELLIGENT OPTIMIZATION OF DRILLING PARAMETERS AND COGNITIVE HUMAN-COMPUTER COOPERATIVE CONTROL BASED ON ADAPTIVE RBF NEURAL NETWORK AND MOPSO

Chaoyan Han [0009-0003-4745-3541], Ailin Sun [0009-0005-6920-6087], Shuo Sun [0009-0002-2059-2122]*
College of Mechanical Engineering, Baoji University of Arts and Sciences, Baoji, 721013, China

Abstract - In modern drilling engineering, there are some problems in optimizing drilling rig process parameters, such as relying on human experience, response lag, etc. Therefore, an intelligent optimization model based on the radial basis function neural network and a panoramic human-computer interaction cooperation architecture are proposed. This study mainly uses the gradient descent method to achieve online updating of network parameters. Meanwhile, a multi-objective particle swarm optimization based on the competition mechanism was designed to optimize process parameters. In addition, this research develops a graphical user interface and a dynamic allocation model of human-machine collaborative control rights that incorporate cognitive engineering. The results showed that the root mean square error of the mechanical penetration rate of the adaptive radial basis function neural network under hard formation conditions was 1.85m/h, and the root mean square error of the mechanical specific energy was 15.80MPa. The improved multi-objective particle swarm optimization had a hypervolume index of 0.8325, and a single optimization time was only 45.6ms. The reconstructed human-machine interaction interface shortened the recognition time from 3.85s to 1.85s in emergency blowout prevention tasks. In summary, the method achieves the Pareto balance of maximizing the mechanical penetration rate, minimizing the mechanical specific energy and optimizing the comprehensive cost. This effectively improves the safety and efficiency of drilling rig operations. The research provides a new paradigm of efficient and safe human-computer collaborative decision-making for intelligent drilling systems in high-pressure and complex environments.

Keywords: Radial basis function, Drilling rig, Human-machine interaction, Multi-objective optimization, Cognitive engineering, Graphical user interface.

1. Introduction

In modern drilling engineering, drill rig operations are faced with extremely complex geological environments and highly nonlinear dynamic conditions. Small changes in process parameters such as drilling pressure, turntable speed and pump displacement will cause severe fluctuations in the underlying mechanical drilling speed and mechanical specific energy [1-3]. In traditional drilling operations, parameter adjustment is highly dependent on the engineering experience of the driller. With the increasing number of drilling tasks, it is difficult to cope with the problems in the process with manual experience alone [4]. Past research tended to establish static physical prediction models or use basic machine learning algorithms for parameter optimization. Although it has achieved certain results, it still has many shortcomings. First of all, the static prediction model responds slowly when faced with sudden changes in formation conditions such as sudden increases in rock hardness, and has serious prediction lags and huge error envelopes [5-6]. Secondly, conventional multi-objective optimization algorithms take a long time for a single calculation and are difficult to meet the needs of high-frequency real-time optimization at the drilling site. Finally, at the human-machine interaction (HMI) level, the traditional matrix-arranged graphical user interface (GUI) ignores cognitive engineering under high-voltage operations, resulting in damage to the electromechanical system [7]. Therefore, this study proposes an intelligent optimization model of process parameters and a panoramic HMI collaborative architecture based on radial basis function (RBF) neural network. It is hoped that this can provide drillers with an efficient and safe intelligent drilling control solution.

dx.doi.org/10.17683/ijomam/issue25/v2.8

2. Related Work

The application of data-driven and machine learning methods in the field of drilling process parameter optimization has gradually become a research hotspot. Yang Z proposed a machine learning-driven optimization method based on adjacent well data to solve the low prediction accuracy of traditional drilling parameter optimization models. This study used field measurable parameters such as weight on bit, rotation speed, flow rate, etc. to build a coupled model. This method reduced the mean square error by 55%, the torque by 25%, and the mechanical drilling speed by 20% [8]. Penget al. found that during the tripping process of deep wells, unexpected vibrations of the drill string increased downhole safety risks. To this end, this study constructed a multi-objective optimization framework that balances drilling efficiency and safety. The optimization program could effectively obtain the optimal tripping parameters under different working conditions, ensuring safety while improving operating efficiency [9]. Amadi et al. proposed an autonomous drilling prediction optimization model based on data-driven and machine learning to solve the traditional drilling relying on manual experience to select parameters. The results showed that the prediction accuracy of derived variables was significantly better than traditional ground parameters, with a correlation coefficient of 0.985 [10].

RBF neural network, with its powerful nonlinear mapping capabilities, has great advantages in handling tasks such as complex engineering parameter prediction. In actual drilling, traditional methods cannot obtain the rock mechanical parameters of any well section. Wei M et al. proposed a data-driven parameter prediction method. First, the study screened the main influencing factors through the Pearson correlation coefficient, then built three machine learning models that integrated these factors and optimized the hyperparameters. The results showed that the RBF neural network had the strongest generalization ability, with a prediction accuracy of 87.69% [11]. Heidari et al. proposed a blockchain-based RBF model to address the difficulty in balancing intrusion detection accuracy and efficiency under dynamic network architecture. The results showed that the model outperformed existing methods on multiple indicators [12]. Siouda et al. proposed a hybrid neural network classifier that combined RBF and extreme learning machines to solve the insufficient big data processing algorithm capabilities in classifying massive biomedical data. Moreover, it used genetic algorithm to optimize the extreme learning machine hidden neurons. The results showed that the accuracy of the model reached 97.38% [13].

In summary, previous research has made significant progress in prediction and optimization of drilling process parameters based on machine learning and data-driven, but there are still many limitations. First, it focuses on improving the accuracy of the underlying prediction algorithm and fails to take into account the cognitive load and HMI efficiency of drillers in high-pressure operating environments. The second is the lack of signal filtering and transmission delay constraints, which can easily cause visual feedback lag. In addition, with the advancement of drilling automation, the importance of human-computer collaboration in complex industrial systems has become increasingly prominent. Recent interdisciplinary research shows that only improving the accuracy of the underlying algorithm while ignoring the cognitive load of the front-end interface is likely to cause automation surprises and operation delays under emergency conditions. However, there are few studies on jointly modeling neural network parameter optimization and operator's cognitive response time [14-16]. This study proposes an intelligent optimization and HMI collaboration framework for drilling rig process parameters based on RBF neural network, to improve the comprehensive safety and efficiency of drilling operations in complex formations.

The innovation of the research is reflected in three aspects. First, in the perception and prediction layer, an online update mechanism of adaptive radial basis function (Adaptive RBF) based on gradient descent is proposed, which solves the serious delay problem of traditional static network when the stratum suddenly changes. Secondly, in the decision-making and optimization layer, a Multi-Objective Particle Swarm Optimization (MOPSO) algorithm with competition mechanism is designed, which is deeply coupled with the forward prediction of RBF to achieve multi-objective millisecond level optimization. Third, in the implementation and interaction layer, it fills the vacuum between intelligent algorithms and human operators, introduces cognitive engineering to reconstruct the interactive interface, and designs a smooth switching mechanism of human-computer control rights with dual threshold hysteresis loops.

These three modules constitute a complete closed-loop framework from accurate data perception to intelligent and efficient decision-making, and then to human-computer safety execution.

3. Proposed Methodology

This study elaborates on the design principles of the core algorithm and human-machine collaborative architecture of the intelligent drilling rig system. First, a multi-objective intelligent optimization model of process parameters based on the Adaptive-RBF neural network is constructed. Then, the improved MOPSO algorithm is applied to achieve Pareto optimization of drilling efficiency. Second, the study designs a panoramic HMI collaborative control system and reconstructs HMI interface based on cognitive engineering.

3.1 Multi-objective Intelligent Optimization Model of Drilling Rig Process Parameters based on RBF Neural Network

- **Nonlinear Coupling Relationship of Drilling Rig Process Parameters and RBF Network Construction**

The drilling process is essentially a complex physical process with multi-variable coupling, nonlinearity and strong time-varying characteristics. Changes in drilling pressure and rotational speed will directly lead to severe fluctuations in mechanical penetration rate and bottom hole specific energy [17-18]. To map the nonlinear relationship between these process parameters and drilling efficiency, this study introduces RBF neural network as a predictor. The topology diagram of the multi-variable nonlinear coupling relationship between the drilling rig's process parameters is shown in Figure 1.

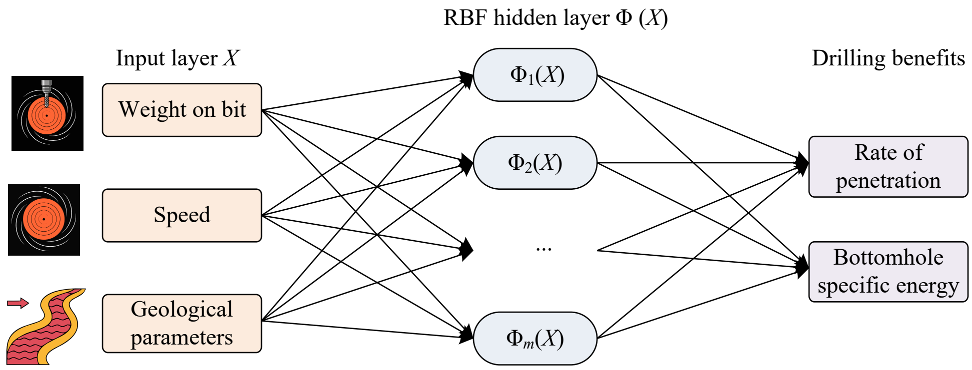

Figure 1: Topological diagram of multivariate nonlinear coupling relationship of drilling process parameters

In Figure 1, input variables such as weight on bit and rotational speed not only interact with each other, but are also affected by the cross-influence of geological environment parameters, which jointly determine the drilling efficiency and energy consumption indicators of the bottom layer. Assuming that the input vector of the RBF neural network contains the currently measured geological parameters and the process parameters to be optimized, denoted as $X=[x_1,x_2,\dots,x_m]^T$, the activation function $\Phi_k(X)$ of the k th hidden layer node is shown in Equation (1) [19].

$$\Phi_k(X)=\exp\left(-\frac{\|X-\mu_k\|^2}{2\sigma_k^2}\right) \tag{1}$$

In Equation (1), $\mu_k=[\mu_{k1},\mu_{k2},\dots,\mu_{km}]^T$ represents the Gaussian base center vector of the k th node in the hidden layer. σ_k is the width parameter that controls the scope of the basis function. $\|\cdot\|$ is the Euclidean norm. By setting reasonable μ_k and σ_k, the network can effectively extract nonlinear characteristics of drilling.

The output end of the RBF neural network is responsible for outputting the predicted drilling status indicators. The output of the network is $\Psi(X)$, as shown in Equation (2).

$$\Psi(X)=\sum_{k=1}^{K}\Omega_k\Phi_k(X)+\xi_{bias} \tag{2}$$

In Equation (2), K is the total number of hidden layer neurons. Ω_k represents the connection weight between the k th hidden layer node and the output layer. ξ_{bias} is the offset compensation term of the network output.

- **Online Identification of Drilling Status and Establishment of Multi-Objective Optimization Function Family**

After establishing the baseline structure and forward spatial mapping relationship of the RBF neural network, the model also needs to have dynamic self-learning and online identification capabilities of parameters. To ensure the real-time approximation accuracy of the RBF neural network during the drilling process, this study used the gradient descent method to perform online adaptive updating of network parameters. It is defined the loss cost function $J_{loss}(t)$ between the predicted output of the system at time t and the actual sensor feedback value $Y_{real}(t)$ is shown in Equation (3).

$$J_{loss}(t) = \frac{1}{2}\left[Y_{real}(t) - \Psi(X,t)\right]^2 \tag{3}$$

Based on Lyapunov stability theory and the gradient steepest descent law, the dynamic iterative update adaptive law design of the output layer weight A is shown in Equation (4).

$$\begin{aligned}&\Omega_k(t+1) = \\ &\Omega_k(t) + \eta_\Omega\left[Y_{real}(t) - \Psi(X,t)\right]\Phi_k(X) + \alpha_\Omega \Delta\Omega_k(t)\end{aligned} \tag{4}$$

In Equation (4), $\eta_\Omega \in (0,1)$ is the weight learning rate. α_Ω is the momentum factor. The expression of $\Delta\Omega_k(t)$ is shown in Equation (5).

$$\Delta\Omega_k(t) = \Omega_k(t) - \Omega_k(t-1) \tag{5}$$

In the same way, the adaptive adjustment law of the hidden layer center μ_k is derived, as shown in Equation (6).

$$\begin{aligned}&\mu_{kj}(t+1) = \\ &\mu_{kj}(t) + \eta_\mu\left[Y_{real}(t) - \Psi(X,t)\right]\Omega_k\Phi_k(X)\frac{x_j - \mu_{kj}(t)}{\sigma_k^2}\end{aligned} \tag{6}$$

In view of the above-mentioned network structure and parameter adaptive update law, this research constructs a complete online identification and prediction framework. The specific structure is shown in Figure 2.

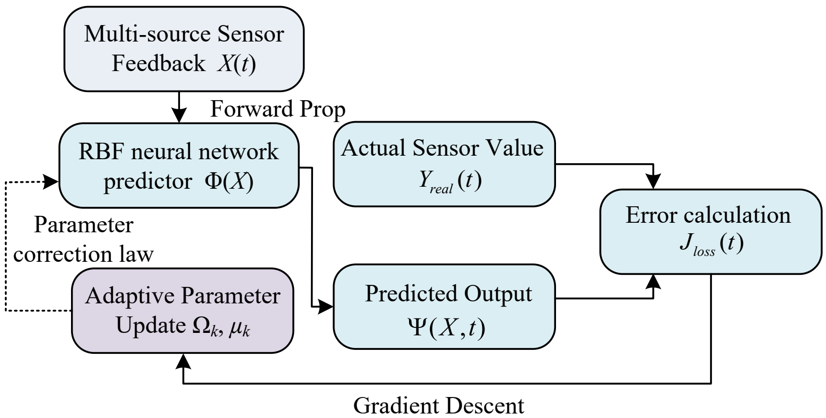

Figure 2: Architecture diagram for online identification and prediction of drilling state parameters

In Figure 2, the online architecture obtains data feedback from front-end multi-source sensors in real time, and uses the calculated prediction error to dynamically reversely adjust the center position of the hidden layer of the network and the output layer weight matrix. After realizing high-precision forward prediction of drilling process parameters, the driller cannot pursue the fastest drilling speed alone, otherwise the drill bit will quickly fail [20-21]. Therefore, this study constructs a drilling multi-objective optimization function family containing three major indicators. The first is the mechanical penetration rate prediction model V_{rop} modified based on rock fragmentation theory, as shown in Equation (7).

$$V_{rop} = \frac{K_{rock}C_{hyd}(F_{wob} - F_{th})^{m_1} N_{rpm}^{m_2}}{1 + \lambda_{wear}H_{wear}} \tag{7}$$

In Equation (7), K_{rock} is the formation drillability characterization coefficient. C_{hyd} is the hydraulic rock clearing efficiency factor. F_{th} is the rock breaking threshold drilling weight of this formation. m_1 and m_2 are the nonlinear indices of the bit weight and rotational speed respectively. λ_{wear} stands for tooth wear sensitivity. H_{wear} is the accumulated wear amount of the current drill bit. Second, to evaluate the energy utilization rate of rock breaking, the study defines the drilling machinery specific energy objective function E_{mse}, as shown in Equation (8).

$$E_{mse} = \frac{F_{wob}}{A_{bit}} + \frac{120\pi \cdot N_{rpm} \cdot M_{torque}}{A_{bit} \cdot V_{rop}} - \eta_{loss} \tag{8}$$

In Equation (8), A_{bit} is the effective cutting cross-sectional area of the drill bit bottom. M_{torque} is the actual output torque feedback value. η_{loss} is the capability attenuation dissipation term. Finally, comprehensively considering time cost and equipment loss, a comprehensive drilling economic cost function C_{total} is established, as shown in Equation (9).

$$C_{total} = \frac{C_{rig}\left(t_{drill} + t_{trip}\right) + C_{bit}}{H_{depth}} \tag{9}$$

In Equation (9), C_{rig} is the drill comprehensive operating fee rate. t_{drill} and t_{trip} represent the actual pure drilling time and tripping time, respectively. C_{bit} is the purchase and depreciation cost of a single drill bit. H_{depth} is the total footage.

- **Parameter Optimization Mechanism based on MOPSO**

To achieve Pareto optimal balance among the three nonlinear objectives, this study introduces MOPSO based on competition mechanism for solution space optimization. The specific calculation, solution, and screening process is shown in Figure 3.

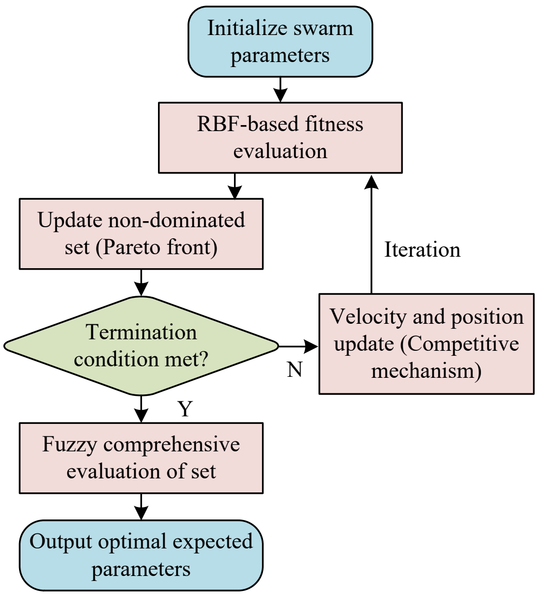

Figure 3: Multi-objective process parameter Pareto frontline optimization flow chart

In Figure 3, the algorithm specifies the particle swarm adaptive fitness evaluation, speed and position update mechanism, and the screening iteration process of non-dominated solution sets. This study uses the above three objective functions as fitness evaluation criteria, combines the real-time nonlinear parameter estimation provided by RBF neural network, and uses the MOPSO algorithm to iteratively search the solution space. Through fuzzy comprehensive evaluation of the Pareto front solution set generated by optimization, the system can independently select the most robust expected values of process parameters under the current working conditions.

3.2 Drilling Rig HMI Collaborative Control and System Implementation

- **Multi-Source Data Filtering and Wireless Communication Delay Modeling**

After obtaining the multi-objective optimal drilling parameters driven by the RBF neural network, it is necessary to explore how to transmit these complex instructions to the driller operator [22-23]. The driller's HMI not only involves the visual display of the GUI, but also includes the preprocessing of underlying sensor data, the transmission of wireless communications, and the allocation of control rights between man and machine under emergency conditions. Due to the strong electromagnetic interference at the drilling site, the raw sensor data is accompanied by a large number of high-frequency burrs. To this end, this study designs a digital filtering algorithm based on the fusion of weighted moving average and first-order lag at the data receiving front end of the interactive system. It is assumed that the original acquisition signal is $D_{raw}(t)$, and the smooth display data $D_{smooth}(t)$ after UI bottom layer preprocessing is defined in Equation (10).

$$D_{smooth}(t) = \beta_{lag} D_{smooth}(t-1) + (1-\beta_{lag})\sum_{i=0}^{W-1}\gamma_i D_{raw}(t-i) \tag{10}$$

In Equation (10), $\beta_{lag} \in [0,1)$ is the first-order inertia lag filter coefficient. W is the width of the sliding window. γ_i is the spatial weight allocation of data within the window and satisfies $\sum\gamma_i = 1$. During the data transmission process, the system uses LoRa wireless spread spectrum communication technology with strong anti-interference ability.

- **Interface Cognitive Engineering Optimization and Dynamic Adaptive Alarm Mechanism**

Considering the cognitive and operational load of drillers under high-intensity continuous operations, this study introduces ergonomics to reconstruct the topology of the driller terminal interactive interface and cognitive hot zone distribution, as shown in Figure 4.

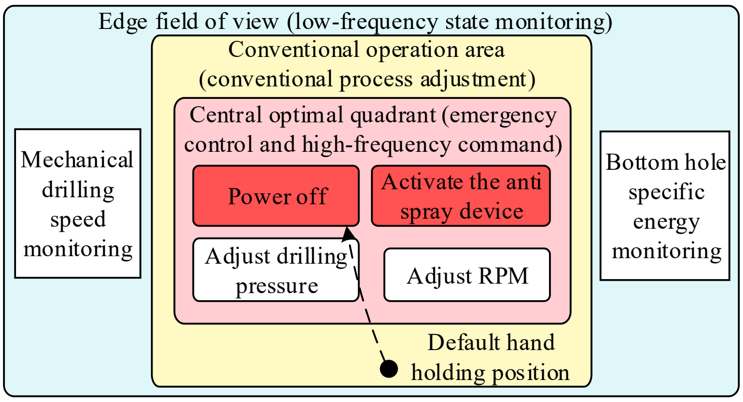

Figure 4: Layout of panoramic HMI interface and visual cognitive hotspot map of the driller terminal

In Figure 4, the system prioritizes the deployment of high-frequency commands and emergency safety buttons in the center of the operator's line of sight and in the optimal quadrant of the hand movement trajectory. At the level of interactive interface design of the drill rig console, this research incorporates the principles of ergonomics and cognitive psychology. In emergency conditions, the driller must quickly perform operations such as cutting off the power supply on the touch screen. To optimize the touch interaction efficiency of the driller, this study introduces a modified Fitts' law model to quantify the operator's interaction time T_{action} from discovering anomalies to completing the click of the screen button, as shown in Equation (11).

$$T_{action} = a_0 + b_0 \log_2\left(1 + \frac{D_{dist}}{W_{target} \cdot \cos(\varphi_{angle})}\right) \tag{11}$$

In Equation (11), a_0 and b_0 are empirical constants that depend on the reaction ability of the driller and the response of the touch screen hardware. D_{dist} is the physical distance from the starting point of the driller's finger to the target button. W_{target} is the effective touch width of the interface control. φ_{angle} is the operation declination compensation between the hand movement trajectory and the screen normal. Meanwhile, the HMI system has a built-in dynamic adaptive alarm mechanism. It is assumed that the current monitoring value of the q key parameter is $P_{mon}^{(q)}$, and its dynamic alarm confidence level S_{alarm} is calculated as shown in Equation (12).

$$S_{alarm} = \exp\left(\lambda_{risk} \cdot \frac{P_{mon}^{(q)} - P_{safe}^{(q)}}{P_{max}^{(q)} - P_{safe}^{(q)}}\right) - 1 \tag{12}$$

In Equation (12), λ_{risk} is the formation risk coefficient. $P_{safe}^{(q)}$ and $P_{max}^{(q)}$ are the dynamic safety baseline and ultimate damage threshold of this parameter respectively. When S_{alarm} exceeds the warning line, the HMI system will not only trigger a red and yellow strobe visual warning, but also link the sound and light alarm module to perform multi-modal warnings. The system data interaction flow and alarm timing are shown in Figure 5.

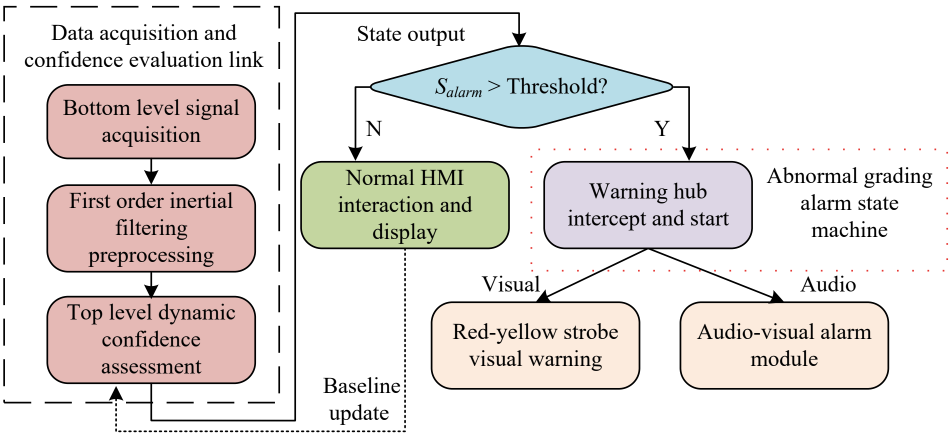

Figure 5: System data interaction flow and alarm timing diagram

Figure 5 shows the complete decision-making link from bottom-level signal acquisition, first-order inertial filtering preprocessing, to top-level dynamic confidence assessment feedback. When the sequential logic register determines that S_{alarm} exceeds the set threshold vector, the early warning center will intercept and start the multi-modal alarm state machine.

- **Dynamic Allocation Model of Human-Machine Collaborative Control Rights**

After calculating the optimal parameters based on the RBF neural network, the system established a set of hybrid collaborative control output models. It is assumed that the process parameter vector recommended by artificial intelligence (AI) is U_{AI}, the instruction vector input by the driller through the console joystick or touch screen is U_{Human}, and the system's final execution instruction U_{Final} adopts a dynamic weight smooth transition strategy, as shown in Equation (13).

$$U_{Final} = \Gamma_{ai} \cdot U_{AI} + (1-\Gamma_{ai}) \cdot U_{Human} \tag{13}$$

In Equation (13), $\Gamma_{ai} \in [0,1]$ is the weight coefficient of AI takeover. If the driller's operation deviates from the safety envelope for a long time, the system will consider the driller to be in a fatigue or misoperation state. The update logic of the confidence variable Γ_{ai} is shown in Equation (14).

$$\frac{d\Gamma_{ai}}{dt} = -\frac{1}{\tau_{blend}}\Gamma_{ai} + \frac{1}{\tau_{blend}} f_{trust}(\Delta U) \tag{14}$$

In Equation (14), τ_{blend} is the smooth transition time constant. $f_{trust}(\Delta U)$ is a nonlinear step mapping function for judging the artificial error $\Delta U = \| U_{AI} - U_{Human} \|$. Combining the artificial confidence dynamic evaluation model and the smooth transition integration algorithm, the dynamic switching state diagram of the drill rig and AI control rights is shown in Figure 6.

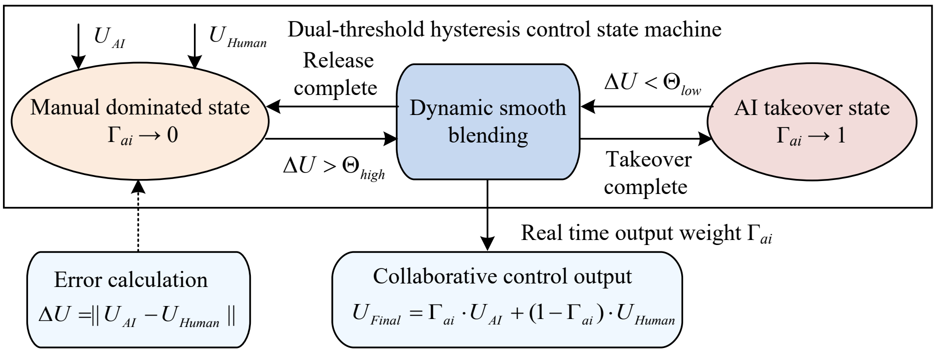

Figure 6: State diagram of dynamic control switching between driller and AI

In Figure 6, the system deeply integrates the Schmitt trigger principle within the control right deprivation and release discriminant function f_{trust}, and has dual-threshold hysteresis loop characteristics.

4. Experiment Setup and Analysis

This study first compares and analyzes the time-varying tracking accuracy and error convergence performance of the Adaptive-RBF neural network under complex and sudden formations, and verifies the advantages of the improved MOPSO algorithm in parameter optimization.

Combined with the driller's simulated operations, the cognitive interaction timeliness of the reconstructed HMI interface is evaluated. Moreover, the effectiveness of the dual-threshold hysteresis loop smooth transition mechanism is verified.

4.1 Experimental Platform and Environment Settings

This study employs the actual drilling historical data set of a large oil field and the dSPACE semi-physical simulation platform to conduct experimental verification of the proposed RBF neural network intelligent optimization algorithm and HMI human-machine collaboration system. The dataset is available for use. The simulation environment is deployed on Intel Core i9-12900K, 64GB RAM, NVIDIA RTX 3090 hardware platform, and the algorithm is written based on Python 3.9 and PyTorch framework.

4.2 Time-varying Tracking and Error Convergence Analysis of Prediction Model

To verify the nonlinear mapping and time-varying tracking capabilities of the Adaptive-RBF neural network based on the gradient descent method for online updating of mechanical penetration rate and mechanical specific energy, this study uses traditional static RBF networks, back propagation neural network (BPNN) and support vector machine (SVM) for comparison.

In Figure 7(a), when drilling to 1050m, the simulated drill bit suddenly drills into the hard formation, and the real mechanical penetration rate is as low as 6.00m/h. BPNN, SVR, and RBF experienced serious prediction lag. The predicted value still remains above 13.85m/h at 1050m, and it is not close to the true curve until 1080m. In contrast, the Adaptive-RBF model responds quickly at 1050m and reaches 6.15m/h at 1052m.

In Figure 7(b), at 1050m, due to the sudden increase in rock hardness, the actual mechanical specific energy required to break unit volume of rock increases from 22.45MPa to 40.00MPa. The static BPNN and SVR models respond slowly after mutation, and the predicted values at 1050m are only 21.50MPa and 22.50MPa. The Adaptive-RBF instantly adjusts to 32.50MPa at 1050m and increases to 39.50MPa at 1052m, showing extremely strong nonlinear dynamic mapping capabilities.

In Figure 7(c), Adaptive-RBF has the lowest Loss, and the Loss drops to 0.4250 at the fifth Epoch, which is much faster than the other three algorithms.

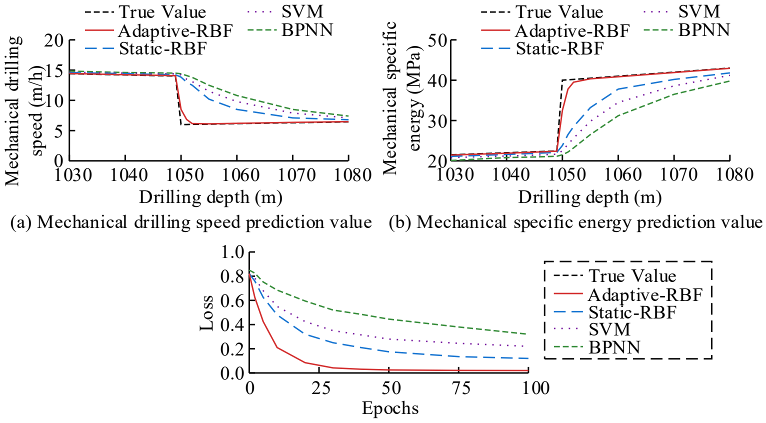

(a) Mechanical drilling speed prediction value (b) Mechanical specific energy prediction value

(c) Algorithm loss convergence curve

Figure 7: Comparison of dynamic tracking and loss convergence of different prediction models

The study then tested the generalization ability and prediction accuracy of each prediction model under different complex stratigraphic conditions, selecting three typical lithology stratigraphic data: soft, medium and hard. The evaluation indicators use root mean square error (RMSE) and mean absolute percentage error (MAPE). In Figure 8(a), in soft formations, the differences between the models are relatively small. In the most complex hard formation conditions, the mechanical penetration rate RMSE of BPNN is increased to 4.88m/h, and the specific energy RMSE is 45.20MPa.

In contrast, the indicators of the Adaptive-RBF model are only 1.85m/h and 15.80MPa respectively. In Figure 8(b), the MAPE values of Adaptive-RBF are lower than those of the other models. From soft formation to hard formation, the ROP MAPE is only 3.45%, 4.88% and 6.15% respectively. After the system introduces the gradient steepest descent law to adjust the hidden layer center in real time, the model can quickly converge the relative prediction error within the extremely low safety threshold allowed by the project.

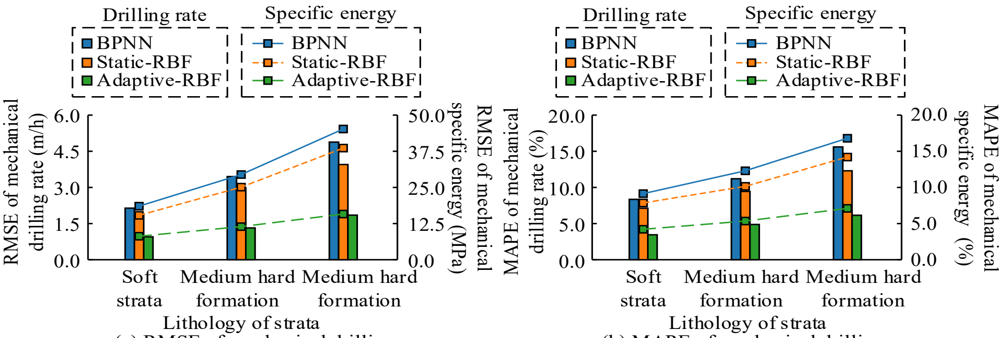

(a) RMSE of mechanical drilling speed and specific energy (b) MAPE of mechanical drilling speed and specific energy

Figure 8: RMSE and MAPE of different models

4.3 Performance Verification of Multi-Objective Process Parameter Optimization Algorithm

This study continues to verify the superiority of the MOPSO algorithm that introduces a competition mechanism in balancing the maximization of mechanical penetration rate, minimization of mechanical specific energy and optimization of drilling costs. The population size is 100 and the maximum number of iterations is 200. Comparison algorithms include non-dominated sorting genetic algorithm II (NSGA-II) with elite strategy, multi-objective artificial bee colony (MOABC) and standard-MOPSO. Hypervolume (HV), generational distance (GD) and spatial evaluation index (spacing, SP) are used for quantitative evaluation. Figure 9(a) shows a set of non-dominated solutions found by the proposed algorithm under three conflicting objectives. The scattered points in the figure form an obvious curved surface, reflecting the mutual constraints between the three indicators. The gradient of the scatter point color from blue to red reflects the changing trend of the ROP from low to high. In Figure 9(b), Proposed-MOPSO has the highest HV, reaching 0.8325±0.005, which is significantly better than the NSGA-II algorithm's 0.6845±0.02 and MOABC's 0.7120±0.01.In Figures 9(c) and 9(d), the GD and SP of Proposed-MOPSO are as low as 0.0125±0.001 and 0.0210±0.001 respectively, which are significantly lower than the 0.0255±0.001 and 0.0415±0.002 of the Standard-MOPSO algorithm.

This shows that the Proposed-MOPSO has obvious advantages in balancing the three conflicting goals of maximizing the mechanical penetration rate, minimizing the mechanical specific energy, and optimizing the drilling cost.

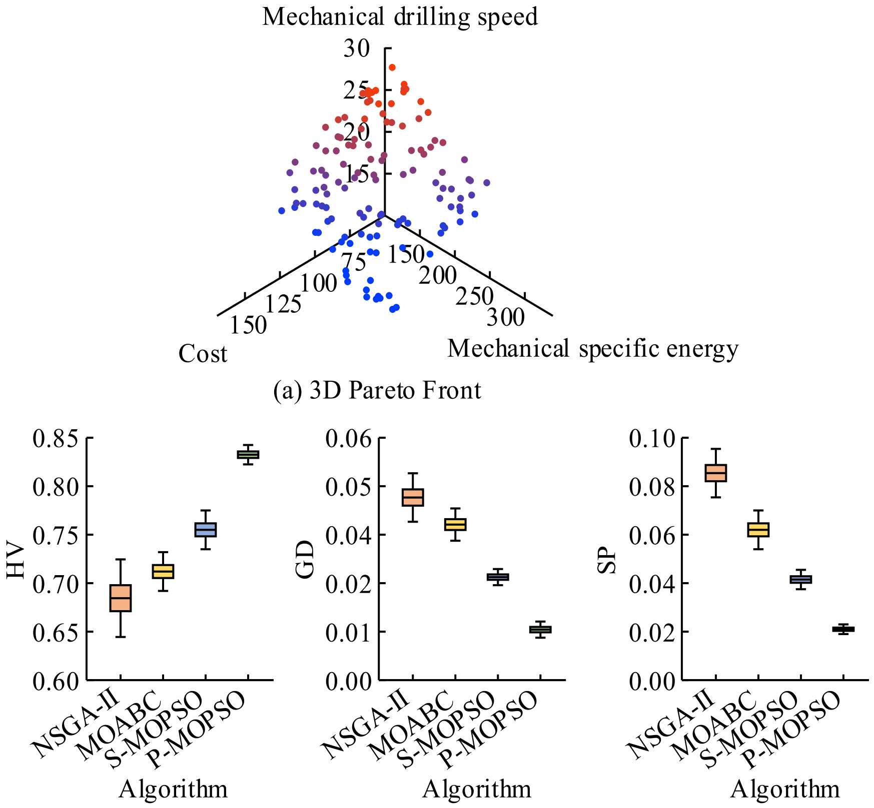

(a) 3D Pareto Front

(b) HV of different algorithms (c) GD of different algorithms (d) SP of different algorithms

Figure 9: Three dimensional Pareto front and performance indicators of different optimization algorithms

This study continues to verify the single optimization time and memory usage of each algorithm. In Figure 10(a), all algorithms have high stability in the 20-cycle test. MOABC's single time consumption is the longest, stable at more than 110ms, and the calculation cost is the highest. Followed by NSGA-II and Standard-MOPSO, the average values are 85.4ms and 68.2ms, respectively, while Proposed-MOPSO is only 45.6ms. In Figure 10(b), the memory footprint of Proposed-MOPSO is only 85.2MB, which is significantly lower than that of other algorithms. This shows that the Proposed-MOPSO algorithm optimizes low-latency computing and lightweight memory.

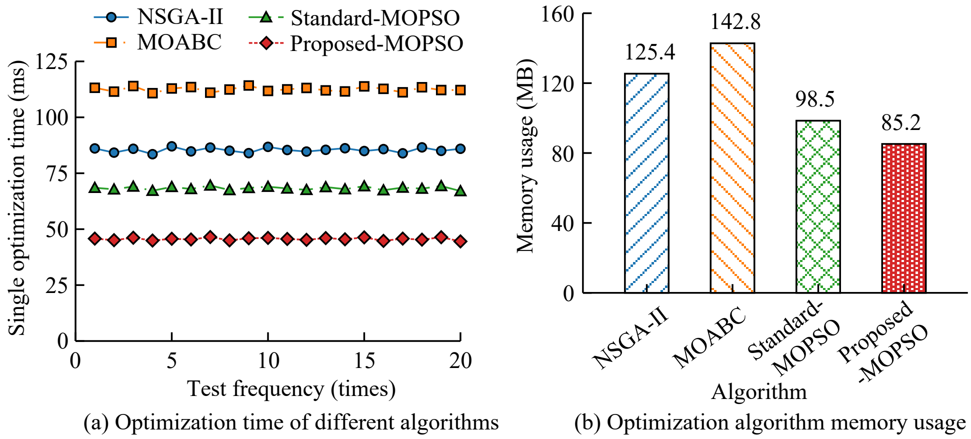

Figure 10: Optimization time and memory usage of different algorithms

4.4 Evaluation of Cognitive Interaction Efficiency of Driller HMI Interface

The study then quantitatively analyzes the time advantage of the driller HMI interface in responding to emergency instructions that incorporates ergonomics and reconstructs cognitive hot zones. The study recruits 15 drillers with more than 5 years of experience. Three types of tasks are set in the simulator: regular parameter adjustment, mild warning processing, and emergency blowout preventer activation. This study compares the interaction time and eye movement hot zone distribution of the traditional matrix-arranged GUI and the reconstructed GUI. In Figure 11(a), the recognition and touch times of the reconstructed GUI are lower than those of the traditional GUI in the three tasks. In emergency blowout prevention tasks, the average recognition time of traditional GUI is as long as 3.85s. The average recognition time of the reconstructed GUI is only 1.85s, and the touch execution time is shortened from 1.85s to 0.80s. In Figure 11(b), under the traditional matrix layout, the eye movement of the driller shows disorderly jumps and large-scale retracements, and high-frequency dwell points are scattered throughout the screen. The visual hot area on the reconstructed GUI screen shows a high degree of central convergence characteristics, which verifies the superiority of this method.

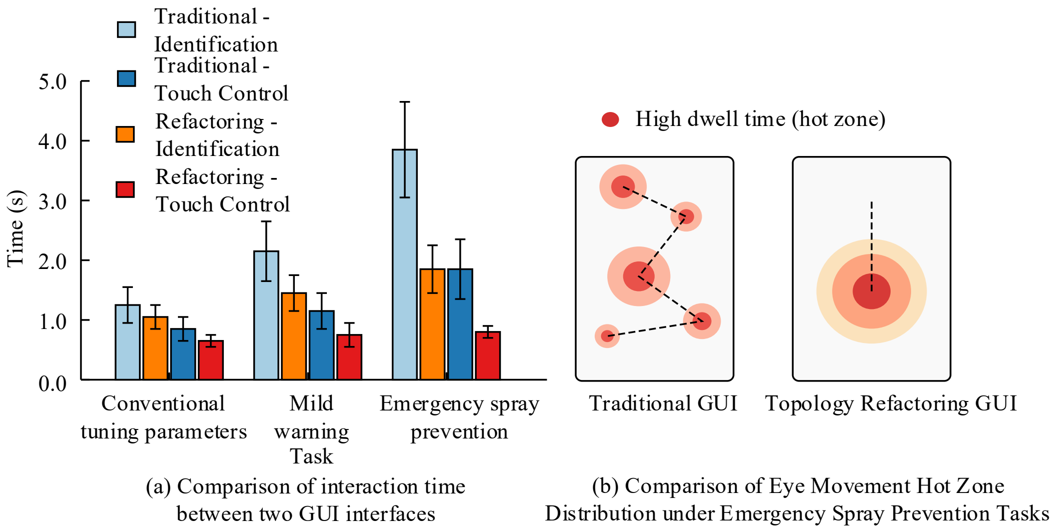

Figure 11: Interaction time and eye movement hotspot distribution of different methods

4.5 Dynamic Allocation and Smooth Transition Verification of Human-Machine Collaborative Control Rights

This study finally verifies the impact of the smooth transition time constant on the human-machine collaborative system and verifies the effectiveness of the Schmitt trigger in suppressing control right oscillations. The system outputs a control power dynamic response curve under the optimal setting of τblend=2.0s. In Figure 12(a), the red solid line represents the manual operation error. At 1.5s, ΔU rises rapidly due to artificially injected step misoperation. When it breaks through the set high threshold upper limit, the AI weight Γai starts to increase in points. At 6.5s, the manual instruction is restored and ΔU drops rapidly. At this time, Γai does not drop immediately. It is not until ΔU is lower than the lower limit of the threshold that control begins to be released smoothly. This dual-threshold design can effectively eliminate frequent control rights grabs that may occur near the 50% error critical point. In Figure 12(b), Uhuman shows extreme artificial step instructions with an amplitude of up to 90%. If a rigid switching of τblend=0.5s is adopted, the electromechanical system will withstand an impact acceleration of up to 15.4m/s2, which can easily cause equipment damage. Ufinal is the collaborative instruction actually output by the system. At the moment when the misoperation occurred, the AI weight had not yet been fully established, resulting in a controllable rising peak in Ufinal. Then, as the AI takes over, the instructions are pulled back to the safe low level set by the bottom layer. This shows that the deep combination of the smooth transition mechanism and the dual-threshold hysteresis loop eliminates high-frequency oscillations during the handover of human-machine control rights, and plays an effective buffering role in extremely dangerous operation instructions.

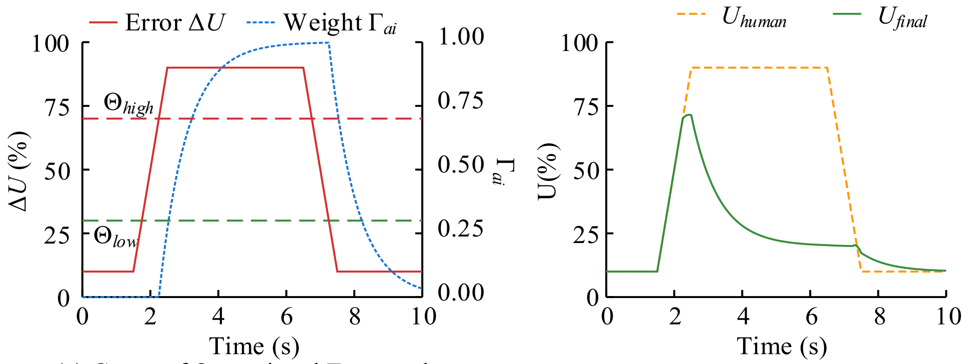

(a) Curve of Operational Error and AI Control Weight over Time

(b) The waveform diagram of the final execution instruction over time

Figure 12: Dynamic response curve of control rights

To further verify the applicability of the proposed intelligent optimization and human-computer cooperation framework under a wider range of drilling conditions, a comprehensive comparison experiment of multiple working conditions was designed. Three typical complex drilling conditions are selected in the experiment: (1) Frequent alternating formation is used to test the dynamic response capability of the system. (2) The deep high-temperature and high-pressure well section is used to test the stability of the model in extreme environments. (3) The extended reach directional well section is used to test the multi-target balance ability under complex friction torque. The research compares the proposed system (Adaptive RBF+MOPSO+Reconstructed Cognitive HMI) with two commonly used benchmark methods in academia. Method A is static BPNN prediction+standard NSGA-II optimization+traditional matrix GUI. Method B is static RBF prediction+standard MOPSO optimization+traditional matrix GUI. The experimental evaluation indicators include the average rate of penetration (ROP), the average mechanical specific energy (MSE), the average human-machine intervention time in emergencies and the comprehensive drilling cost saving rate.

The specific experimental data are shown in Table 1. From Table 1, in the frequently alternating stratum, due to the high frequency mutation of rock hardness, the ROP improvement of Method A and Method B is limited due to the lack of online update mechanism. The system proposed in the study benefits from the adaptive RBF's parameter online identification ability, with ROP reaching 11.45 m/h and MSE dropping to the lowest 35.20 MPa. In extended reach directional wells and high temperature and high pressure deep wells, the improved MOPSO algorithm effectively jumps out of the local optimum through the competition mechanism, resulting in the comprehensive cost savings of 14.2% and 12.8%, respectively. Finally, because the proposed method integrates the HMI interface of cognitive engineering reconstruction and the dual threshold control right allocation mechanism, the response time of human-machine intervention is stably controlled between 1.15s and 1.45s, which is significantly better than that of the comparison method. The deep integration of machine learning optimization algorithm and cognitive human-computer interaction can effectively break the bottleneck of single underlying algorithm optimization.

Table 1: Comparison of comprehensive performance of each system under different drilling conditions

Drilling Conditions	Methods	ROP (m/h)	MSE (MPa)	Intervention Time (s)	Cost Saving Rate (%)
Interbedded Formation	Method A	8.25	48.5	3.55	5.2
	Method B	9.4	42.15	3.42	8.5
	Proposed System	11.45	35.2	1.15	15.4
HPHT Deep Well	Method A	4.5	65.2	4.1	3.1
	Method B	5.25	58.4	3.85	6.4
	Proposed System	6.85	49.55	1.45	12.8
Highly Deviated Well	Method A	6.1	55.45	3.8	4.5
	Method B	7.35	49.2	3.5	7.6
	Proposed System	9.2	41.8	1.25	14.2

5. Conclusions

This study constructed an intelligent optimization model based on the RBF neural network and a panoramic HMI collaborative architecture. The results showed that the ROP MAPE of the Adaptive-RBF neural network from soft formation to hard formation was only 3.45%, 4.88%, and 6.15%, respectively, which was better than that of the BPNN and SVM models. This was mainly due to the real-time adaptive update mechanism of network parameters driven by the gradient descent method, which effectively eliminated the prediction lag problem of the static model. Meanwhile, the HV of the Proposed-MOPSO algorithm reached 0.8325, the GD and SP were 0.0125 and 0.0210, respectively, and the memory usage was only 85.2MB, which was better than the comparison algorithm. In terms of HMI, the touch execution time of the reconstructed GUI in the emergency blowout prevention task was shortened from 1.85s to 0.80s, and the eye movement hot zone showed a high degree of center convergence. This method had effectively improved the safety and efficiency of drilling operations in complex formations. However, the gradient descent update law of the Adaptive-RBF neural network is sensitive to the initial learning rate, and convergence oscillations may occur under extreme working conditions. Future research will explore adaptive learning rate adjustment strategies to further improve the robustness and adaptive capabilities of the drill rig's intelligent control.

Fundings

The research is supported by 2024 Shaanxi Province Science and Technology Plan Project (Industry University Research Collaboration Innovation Plan): "Intelligent Design and Development of ZJ120 Drilling Machine Driller's Room (Project Number: 2024ZG-YFBT-36-02).

References

[1] Yao, N., Wei, H., Zhang, J., Lu, C., Li, H., Yao, Y.F., Ke, Y.G., & Zhang Y.Z. (2023). Intelligent optimization method for tunnel rotary drilling based on drill string status estimation. *Coal Geology & Exploration*, 51(11), 141-148. https://doi.org/10.12363/issn.1001-1986.23.06.0329

[2] Gan, C., Cao, W.H., Liu, K.Z., & Wu, M. (2023). Dynamic optimization-based intelligent control system for drilling rate of penetration (ROP): Simulation and industrial application. *IEEE Transactions on Industrial Informatics*, 20(3), 3695-3702. https://doi.org/10.1109/TII.2023.3313633

[3] Liu, W., Tan, B., Qian, H., Chen, X., Zhang, Z., Zhang, F., Lin, C., & Jin, L. (2024). A smart driller pilot system for future automatic drilling. *Petroleum Science and Technology*, 42(25), 3981-4004. https://doi.org/10.1080/10916466.2023.2271520

[4] Qiao, Y., Xu, H.M., Zhou, W.J., Peng, B., Hu, B., & Guo, X. (2023). A BiGRU joint optimized attention network for recognition of drilling condition. *Petroleum Science*, 20(6), 3624-3637. https://doi.org/10.1016/j.petsci.2023.05.021

[5] Amer, M.Y., Salem, A.M., Farahat, M.S., & Elsayed, S.K. (2025). Reducing drilling cost in geothermal wells by drilling technology optimization. *Journal of Mining and Environment*, 16(3), 767-788. https://doi.org/10.22044/jme.2025.14206.2647

[6] Brantson, E.T., Adu-Awuku, J., Asase, W., Obeng, S.D.A., Kwakye-Tannor, M.B., Nuamah, J.A., Aboagye, E., Appiah-Adjei, F., Nuetor, F.D., & Opoku, P. (2025). Optimization of well trajectory with machine learning algorithms for geosteering directional drilling. *Journal of Geophysics and Engineering*, 22(5), 1245-1265. https://doi.org/10.1093/jge/gxaf055

[7] Li, F., Wu, J., Chen, J., Peng, H., & Fan, Y. (2023). ELF-EM signal processing while drilling based on human-computer interaction combined

algorithm. *China Communications*, 20(6), 178-198. https://doi.org/10.23919/JCC.2023.00.028

[8] Yang, Z., Liu, Y., Qin, X., Dou, Z., Yang, G., Lv, J., & Hu, Y. (2023). Optimization of drilling parameters of target wells based on machine learning and data analysis. *Arabian Journal for Science and Engineering*, 48(7), 9069-9084. https://doi.org/10.1007/s13369-022-07103-x

[9] Peng, X., Yue, B., Li, G., Qiu, Z., & Yang, H. (2024). Modeling and multi-objective optimization of a drill-string system in the tripping operation. *Nonlinear Dynamics*, 112(24), 21849-21866. https://doi.org/10.1007/s11071-024-10196-8

[10] Amadi, K., Iyalla, I., Prabhu, R., Alsaba, M., & Waly, M. (2023). Development of predictive optimization model for autonomous rotary drilling system using machine learning approach. *Journal of Petroleum Exploration and Production Technology*, 13(10), 2049-2062. https://doi.org/10.1007/s13202-023-01656-9

[11] Wei, M., Qiu, D., Yue, T., Duan, Y., & Wang, H. (2025). New method prediction of rock mechanics parameters in drilling process based on machine learning. *Petroleum Science and Technology*, 43(4), 360-383. https://doi.org/10.1080/10916466.2023.2298998

[12] Heidari, A., Navimipour, N.J., & Unal, M. (2023). A secure intrusion detection platform using blockchain and radial basis function neural networks for internet of drone. *IEEE Internet of Things Journal*, 10(10), 8445-8454. https://doi.org/10.1109/JIOT.2023.3237661

[13] Siouda, R., Nemissi, M., & Seridi, H. (2024). Diverse activation functions based-hybrid RBF-ELM neural network for medical classification. *Evolutionary Intelligence*, 17(2), 829-845. https://doi.org/10.1007/s12065-022-00758-3

[14] Bergh, L. I. V., Teigen, K. S., & Dørum, F. (2024). Human performance and automated operations: a regulatory perspective. Ergonomics, 67(6), 744-758. https://doi.org/10.1080/00140139.2024.2321457

[15] Grindley, B., Parnell, K. J., Cherett, T., Scanlan, J., & Plant, K. L. (2025). Understanding the human factors challenge of handover between levels of automation for uncrewed air systems: a systematic literature review. Transportation Planning and Technology, 48(6), 1383-1408. https://doi.org/10.1080/03081060.2024.2375645

[16] Vempati, L., Gawron, V. J., & Winter, S. R. (2024). Advanced Air Mobility: Systematic review of human factors' scientific publications and policy. Journal of Air Transportation, 32(1), 22-33. https://doi.org/10.2514/1.D0366

[17] Rana, A., Gond, A.K., Rakshit, C., Kumar, S., & Sawmliana, C. (2025). Minimum invasive drill-and-blast designs for optimizing pull efficiency and minimizing overbreaks/underbreaks in varying rock masse. *Geomechanics and Tunnelling*, 18(3), 218-224. https://doi.org/10.1002/geot.202400061

[18] Elahifar, B., & Hosseini, E. (2024). A new approach for real-time prediction of stick–slip vibrations enhancement using model agnostic and supervised machine learning: A case study of Norwegian continental shelf. *Journal of Petroleum Exploration and Production Technology*, 14(1), 175-201. https://doi.org/10.1007/s13202-023-01691-6

[19] Sheikh Khozani, Z., Ehteram, M., Mohtar, W.H.M.W., Achite, M., & Chau, K.W. (2023). Convolutional neural network–multi-kernel radial basis function neural network–salp swarm algorithm: A new machine learning model for predicting effluent quality parameter. *Environmental Science and Pollution Research*, 30(44), 99362-99379. https://doi.org/10.1007/s11356-023-29406-8

[20] Wanasinghe, T.R., Gosine, R.G, Petersen, B.K., & Warrian, P.J. (2023). Digitalization and the future of employment: A case study on the Canadian offshore oil and gas drilling occupation. *IEEE Transactions on Automation Science and Engineering*, 21(2), 1661-1681. https://doi.org/10.1109/TASE.2023.3238971

[21] Du, H., Chan, L., Tong, J., Raad, R., Naghdy, F., Guo, Q., Yu, Y.G., Islam, M.R., Tubbal, F., Ros, M., Li, Z., & Ritz, C. (2025). Industrial progress of robotic automation in mining applications: A survey. *Mining, Metallurgy & Exploration*, 42(2), 537-556. https://doi.org/10.1007/s42461-025-01219-y

[22] Waqas, M., & Naseem, A. (2025). Artificial intelligence in sustainable industrial transformation: A comparative study of industry 4.0 and industry 5.0. *FinTech and Sustainable Innovation*, 1, A2-A2. https://doi.org/10.47852/bonviewFSI52025321

[23] Zhoubeier, G. (2024). Design of UWB-based positioning system for rotary drill. *Academic Journal of Engineering and Technology Science*, 7(5), 67-72. https://doi.org/10.25236/AJETS.2024.070509